1973, *Astron. Astrophys. Suppl.* 8, 505–516.

STUDIES OF FOUR REGIONS FOR USE AS STANDARDS IN 21-cm OBSERVATIONS

DAVID R. W. WILLIAMS
Radio Astronomy Laboratory, University of California, Berkeley

Received May 26, 1972

Four 21-cm regions including three I.A.U. recommended standards have been studied for suitability as standard regions. Maps are presented of the regions of both peak temperatures and integrated intensity. Correction curves are given to convert the measured antenna temperature into the more meaningful brightness temperature. These curves have been derived using detailed measurements of the 85-foot telescope antenna pattern and assuming source brightness distributions of simple form.

Key words: 21 centimeters, standards, calibrations, maps.

INTRODUCTION

The purpose of the present study is to establish absolute brightness temperatures in the 21 cm line for several areas of the sky designated as standard regions. There are various uses for such standard regions: (i) their observation permits the brightness temperature scales of HI surveys to be intercompared, (ii) they provide a convenient means of checking the internal calibration of the equipment on a day-to-day basis and (iii) they provide a means of calibrating an antenna-receiver system.

Three standard fields have been recommended by the I.A.U. (van Woerden (1970)). The primary standard region S8($\ell = 207°$, $b = -15°$) has been used in several surveys including the extensive Berkeley Survey (Weaver and Williams, 1973); S7($\ell = 132°$, $b = -1°$) and S9($\ell = 356°$, $b = -4°$) have been recommended as secondary standards, and one other region S6($\ell = 1.91$, $b = 41.42$) has been studied for suitability as a standard region.

The problem of determining the absolute intensity scale for 21 cm line measurements is a special one since the HI clouds are normally extended with respect to the antenna beam solid angle. In order to estimate the brightness temperatures of the extended standard regions considered here we have (i) mapped the source distributions of the areas of interest, and (ii) measured in detail the antenna pattern of the 85-foot telescope used for the observations. The first of these observations directly provides for each area investigated an antenna temperature, T_A, the scale of which is established by means of a noise tube source calibrated against a hot-cold load in the laboratory. We discuss questions related to the determination of T_A in the first part of this investigation.

For many discussions brightness temperature, T_B, is of more fundamental astrophysical importance than antenna temperature. Observers intercomparing their results with those of others, for example, should compare T_B values rather than T_A values. The first of these, T_B, represents brightness on the sky; the other, T_A, represents that quantity modified by the properties of the telescope, and thus must be different from one set of observations to another.

To transform the observed T_A to T_B one must have knowledge of various source and antenna properties. Limitations of our knowledge of source properties will always impose a limit on the accuracy of the transformation that can be achieved. An important criterion for choice of a standard region to serve as a source for comparison and standardization for all observers is that it should permit transformation from T_A to T_B with maximum accuracy. We discuss transformation problems in the second part of this paper.

RECEIVING EQUIPMENT

The 21-cm line observations at the Hat Creek observatory have been made with the 85-foot telescope and the 100-channel receiver, which have been described earlier (Weaver, et al., 1968). The antenna beam of the 85-foot telescope is of circular cross section; the HPBW for 1420.4 MHz is 35 arc minutes. The crystal filters employed in the 100-channel receiver produced individual contiguous information channels of essentially square bandpass each of 10 kHz bandwidth. The antenna-receiver system is completely automated so that the observation of line profiles proceeds automatically through a series of prescribed grid points on the sky. The telescope is pointed in ℓ and b coordinates precessed to date and corrected for atmospheric refraction and instrumental flexure; the radial velocity with respect to the local standard of rest is computed and the corresponding frequency is entered into the receiver local oscillator so that a given channel "observes" a given velocity. Integration then proceeds for a preset time after which the outputs of the 100 channels are read onto the magnetic tape for processing later. The profiles are calibrated using the internal noise-tube calibration system. The recorded data are then subsequently analyzed using an elaborate reduction procedure which scales the profiles into corrected antenna temperature units and removes a linear baseline. Series of observations made in this manner are presented here in the form of profiles and contour maps.

THE REGIONS INVESTIGATED

Four regions have been studied. The primary standard region S8 shows in its spectrum only the single peak characteristic of the Orion complex which is widely distributed in angle. Region S7 involves the Perseus-arm peak in the profile, which is flat topped and which has a distribution in the sky of large angular extent. Regions S7 and S8 were introduced by the Leiden observers and have been used extensively for calibrations. S8 has been used daily at the Hat Creek observatory as a standard against which the receiver noise calibration system is measured. Region S9 has been used as a standard at Parkes. Region S6 has been studied by Goldstein (1964). Although S6 has not been recommended as a standard by the I.A.U. it does have a single narrow peak which is reported to change only slowly with position in the sky, and may therefore be useful for some purposes.

The coordinates of the four regions are given in Table 1.

Table I
Positions of Regions Observed

Region	Galactic coordinates ℓ	b	R.A. (1950)	Dec. (1950)
S6	1°.91	+41°.42	$15^h\ 28^m\ 58^s$	− 2° 15′
S7	132°.00	− 1°.00	$2^h\ 2^m\ 38^s$	60° 19′
S8	207°.00	−15°.00	$5^h\ 44^m\ 50^s$	− 1° 41′
S9	356°.00	− 4°.00	$17^h\ 48^m\ 46^s$	−34° 25′

Note: S6 is assumed to be $\ell^I = 330°.0$; $b^I = +40°.0$.

OBSERVED PROFILES AND CONTOUR MAPS

HI profiles for regions S6–S9 (observed with a 10 kHz resolution and sampled every 5 kHz) are shown in Figure 1. Units in the figures are measured antenna temperature, T_A in °K, corrected for atmospheric extinction, and velocity measured with respect to the local standard of rest. Table II lists the observed peak antenna temperatures of the lines and the derived integrated line strengths $I = \int_{v_1}^{v_2} T_A(v)\, dv$, evaluated over the indicated velocity limits.

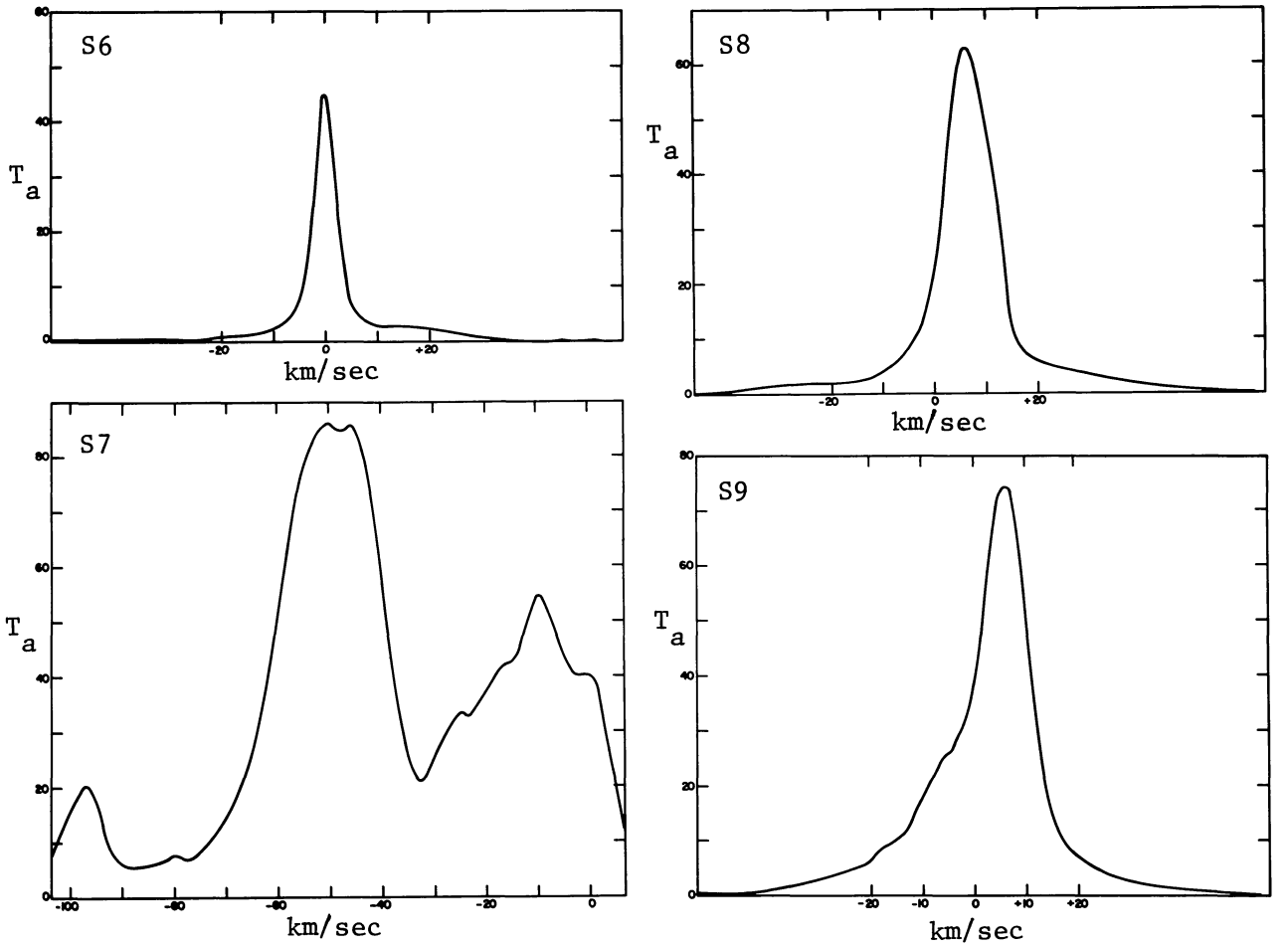

Figure 1. Profiles of the regions. Observed antenna temperatures in °K versus velocity in km/sec. Observing bandwidth is 10 kHz.

Table II
Observed Parameters of the Standard Regions

Region	Peak value of T_A (°K)	Velocity of peak (approx) (km/sec)	Integral (°K km/sec)	Velocity range used for integral (km/sec)
S6 (not I.A.U.)	45	0	261	− 5.8 to + 4.8
S7 I.A.U.	85 to 86.5	−45 to −55	957	−56.3 to −45.8
S8 I.A.U.	63	+7	783	− 4.6 to +21.75
S9 I.A.U.	74	+6	832	1.05 to +14.75

HI profiles have been observed every 0°.25 (15′ arc) in ℓ and b coordinates over an area of 2° × 2° centered on each standard region. Observations are thus spaced slightly less than the one half-beamwidth (17′.6 arc) required by the sampling theorem. The data are presented as computer produced contour maps shown in Figures 2–5 for the four regions. Contour maps (a) and (b) show for each region the distribution on the sky of the peak temperature T_A recorded in the central two channels (each of 10 kHz bandwidth, spaced 5 kHz) centered at the indicated velocities. Contour maps (c) show the distribution of T_A for the average of maps (a) and (b) and correspond to a total observing bandwidth of 15 kHz. Contour maps (d) (for each region) show the distribution of the integral over the velocity limits indicated and over the same area of sky. In maps (d) we have normalized the plot to the value 100 at the center and contours are shown at each 2 percent change in level.

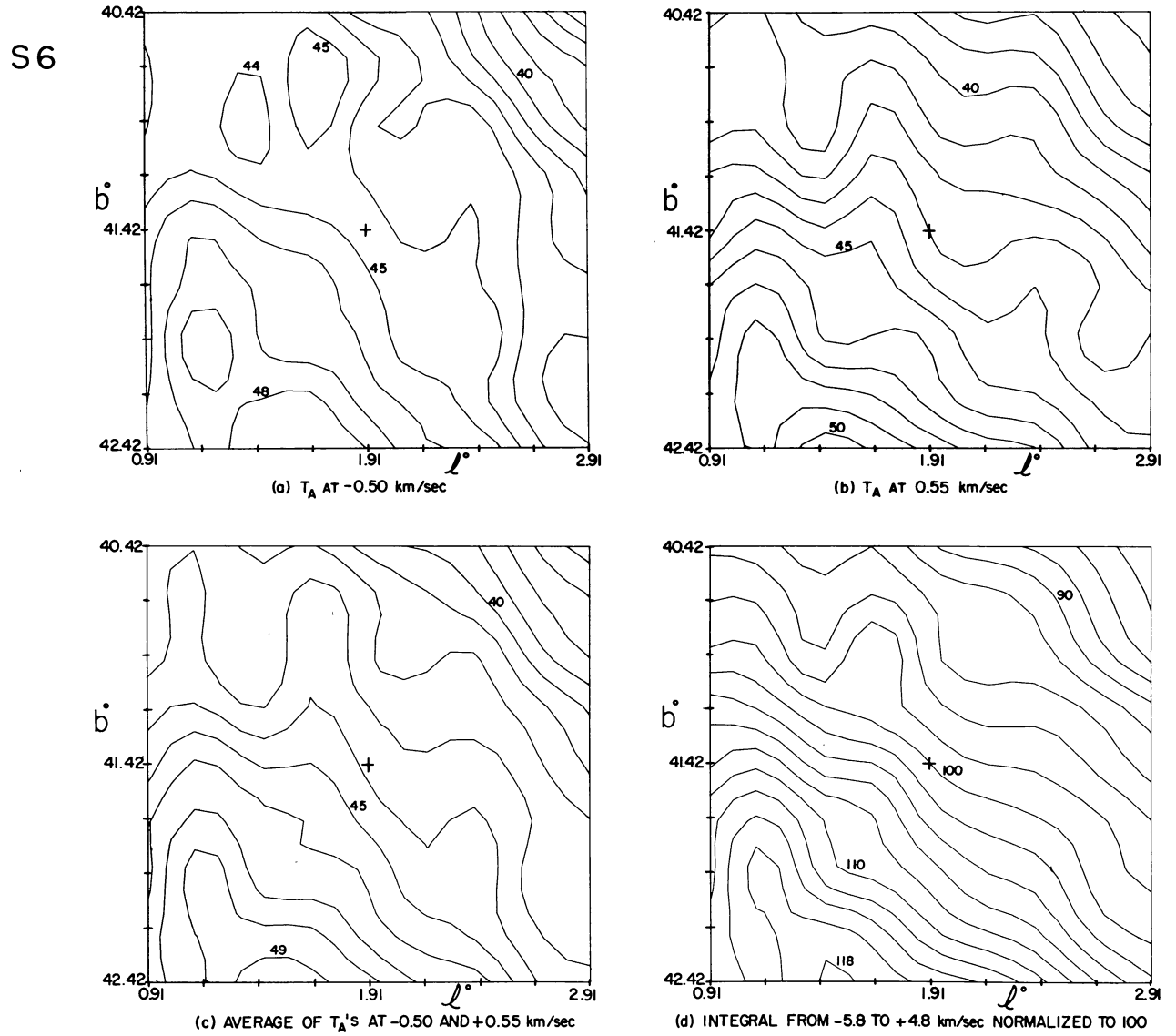

Figure 2. Contour maps centered on region S6 in galactic coordinates ℓ and b. Maps (a) and (b) are the antenna temperatures in °K observed at the stated velocities with a 10 kHz resolution. Map (c) is the averaged antenna temperature of (a) and (b). Map (d) is the integrated intensity normalized to 100 units at the center; the integration is taken over the indicated velocity range.

S7

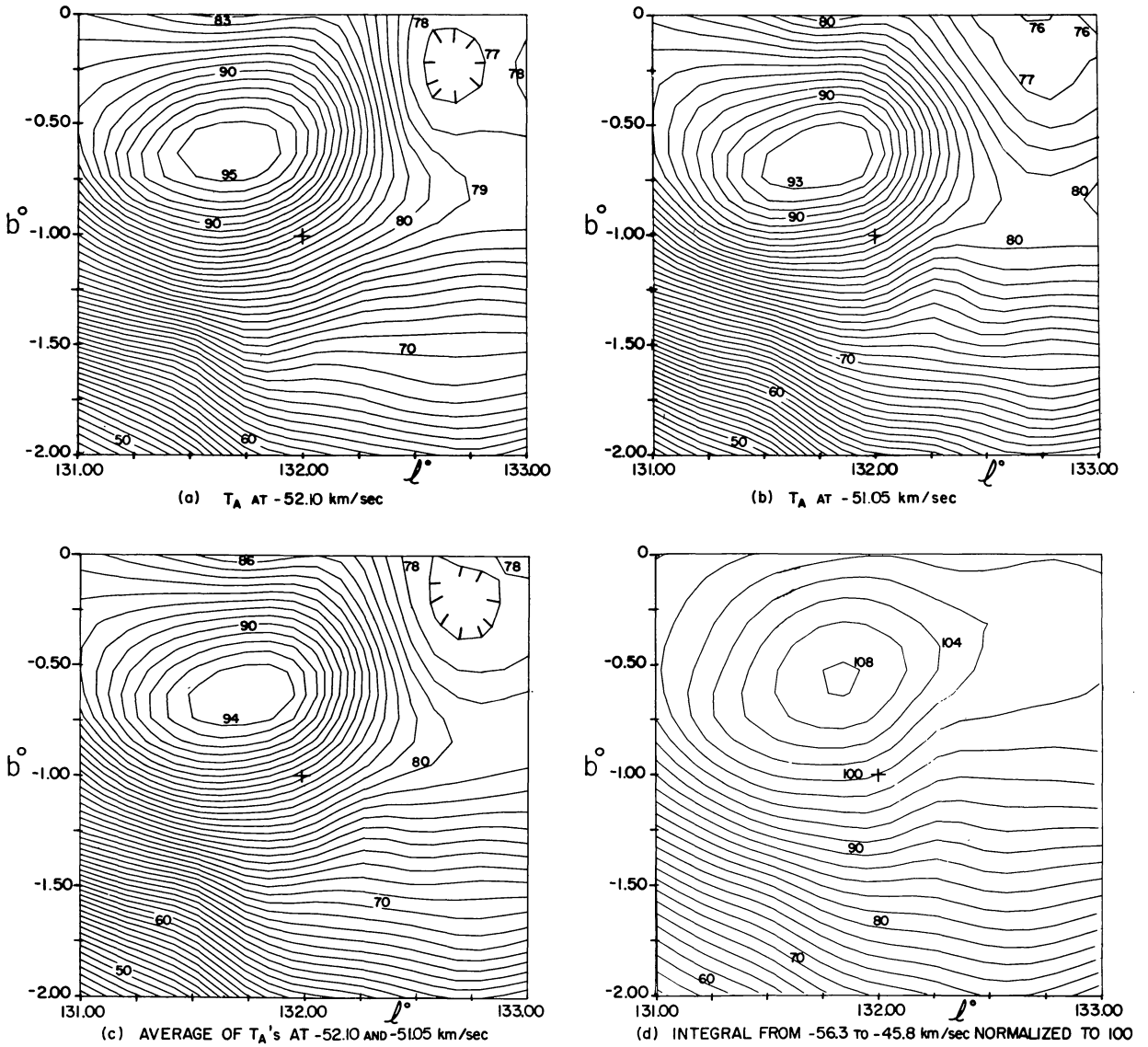

Figure 3. Contour maps centered on region S7 in galactic coordinates ℓ and b. Maps (a) and (b) are the antenna temperatures in °K observed at the stated velocities with a 10 kHz resolution. Map (c) is the averaged antenna temperatures of (a) and (b). Map (d) is the integrated intensity normalized to 100 units at the center; the integration is taken over the indicated velocity range.

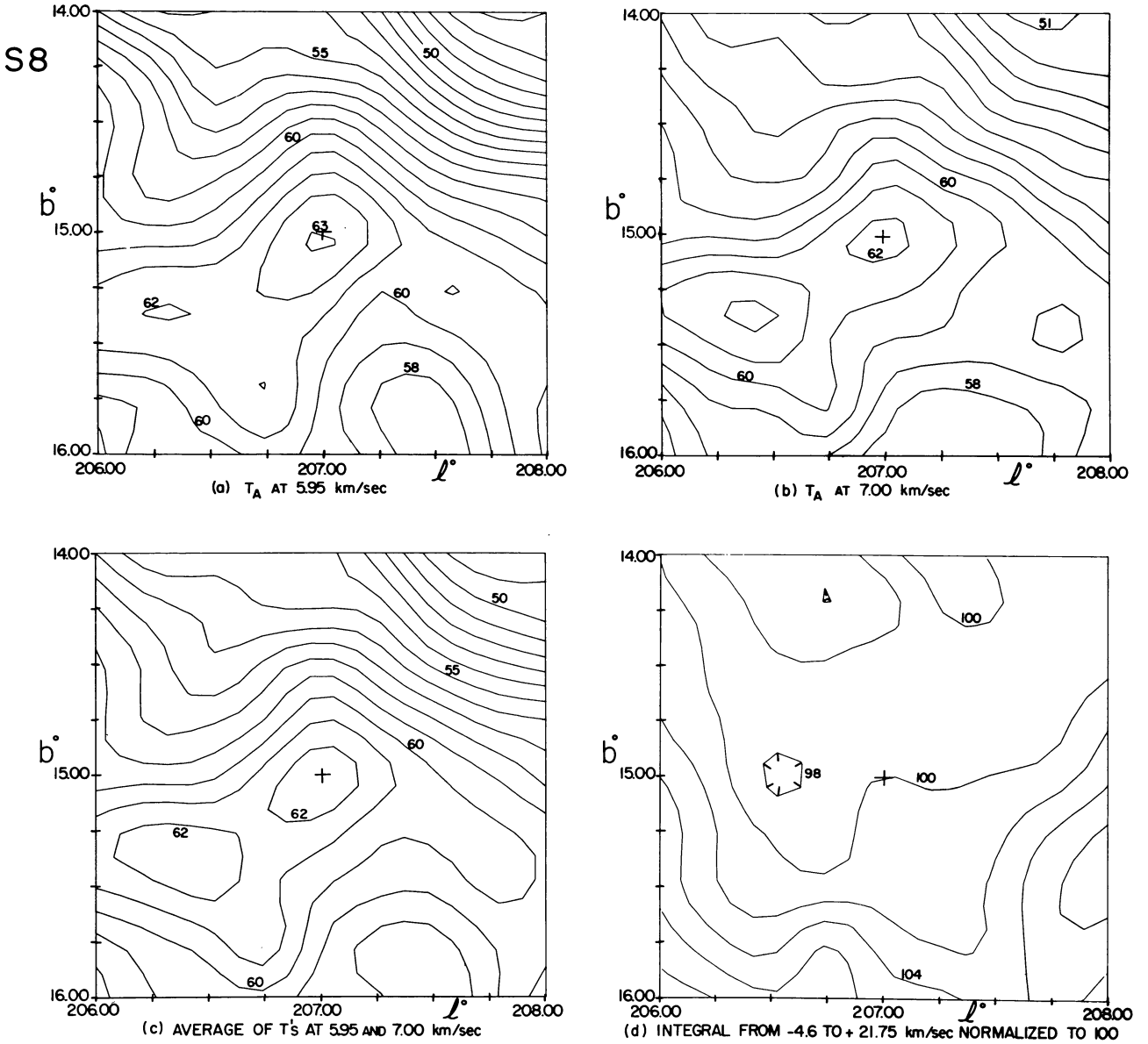

Figure 4. Contour maps centered on region S8 in galactic coordinates ℓ and b. Maps (a) and (b) are the antenna temperatures in °K observed at the stated velocities with a 10 kHz resolution. Map (c) is the averaged antenna temperatures of (a) and (b). Map (d) is the integrated intensity normalized to 100 units at the center; the integration is taken over the indicated velocity range.

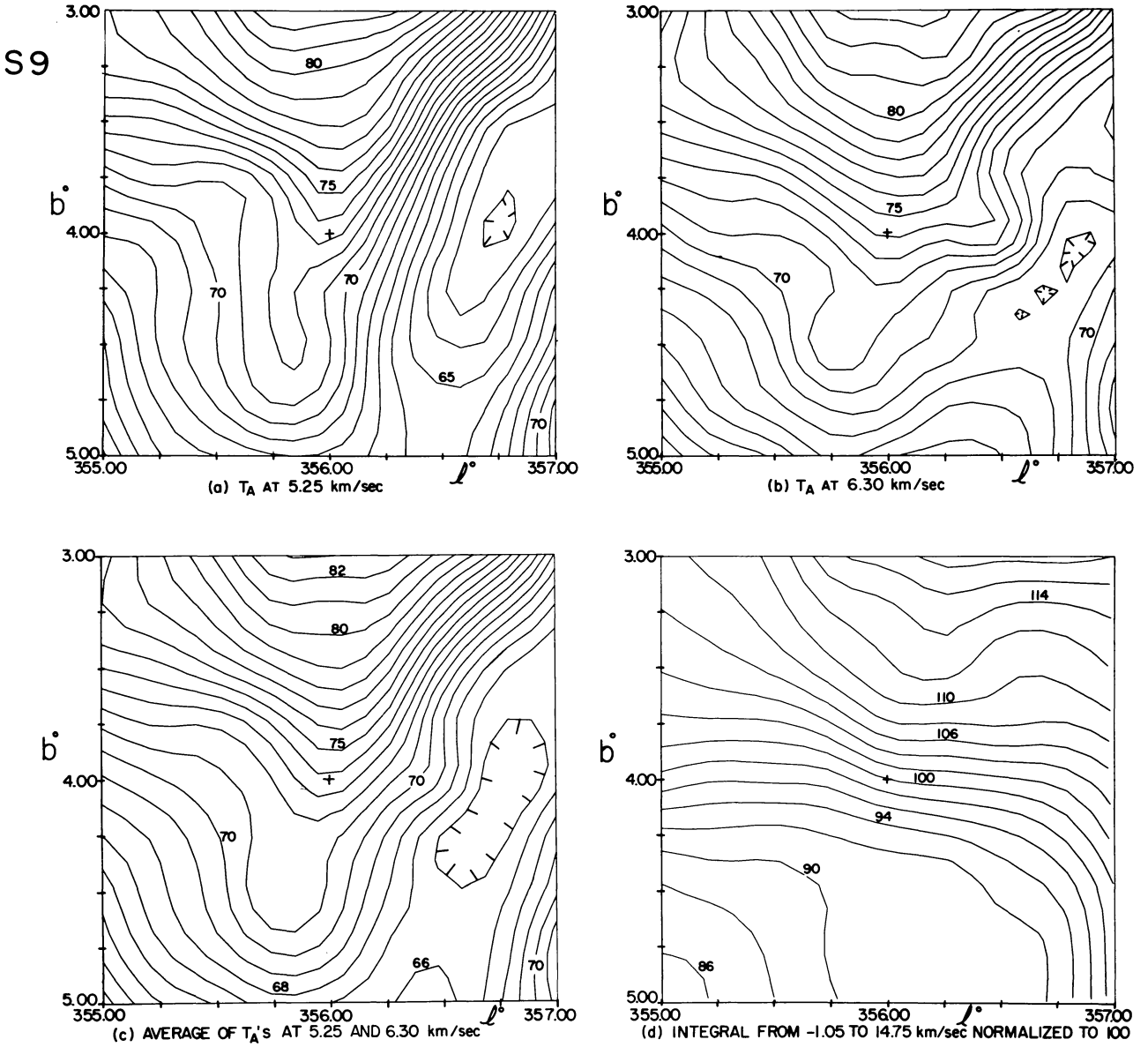

Figure 5. Contour maps centered on region S9 in galactic coordinates ℓ and b. Maps (a) and (b) are the antenna temperatures in °K observed at the stated velocities with a 10kHz resolution. Map (c) is the averaged antenna temperatures of (a) and (b). Map (d) is the integrated intensity normalized to 100 units at the center; the integration is taken over the indicated velocity range.

DISCUSSION OF THE MAPS

Over an area of 0°.5 diameter region S6 shows a 5 percent variation in the peak temperature and a 10 percent variation in the integral. The value of the integral is the smallest of the four regions by a factor of three, and in this regard this region is least suitable in terms of signal-to-noise ratio in a given observing time.

Region S7 has much stronger gradients than any of the others. The top of the profile is resolved into a double peak as shown in Figure 1. Moving the center over to $\ell = 131.75$ and $b = -0°.65$ instead of 132° and −1° would reduce the peak temperature variation to 4 percent over a 0°.5 diameter. Variation in the integral is only 3 percent over the same area. The listed position does not appear to be optimal.

In region S8 the peak temperature varies only 2½ percent over an area 0°.5 diameter and the integral varies only 1 percent over the same area. In this regard S8 is the best region we have observed.

Region S9 shows a gradient in peak temperature of 10 percent over an area 0°.5 diameter. The integrated intensity varies 15 percent over the same area.

In summary, when all the above factors are considered, S8 is probably the most suitable of the four for a standard region; it has been used extensively as a standard in 21-cm survey work at Hat Creek. Regions S6, S7 and S9 are about equally good, provided the S7 central coordinates are moved.

THE EFFECT OF TELESCOPE POINTING AND INSTRUMENTAL BANDWIDTH

The angular size of the regions is large compared to the antenna beam, consequently the small (±1′ arc) positioning errors of the telescope with which our observations were made have no significant effect on the recorded line intensities. The possibility exists, of course, that telescopes of extremely high resolving power will reveal sharp gradients that have been smoothed in the present beam pattern.

The effect of finite instrumental bandwidth on the peak intensity of the profiles shows up typically as a 1–2 percent lowering of the recorded peak temperature in going from 10 kHz to 15 kHz resolution, i.e. from either maps (a) or (b) to map (c). However, the effect of bandwidth on the integrated line strengths, shown in maps (d), is negligible and this is a further argument in favor of using the integral value for intercomparison purposes.

ATMOSPHERIC EXTINCTION CORRECTIONS

The measurements of the S8 profile integrated intensity, which we observed on a daily basis but at varying hour angles, necessitated that corrections be made for the atmospheric extinction at varying zenith distances. Our extensive data plus a separate series made when S8 was close to the horizon led to a reliable determination of the numerical value of the extinction coefficient κ in the expression $T_{A,\mathrm{obs}}(A) = T_A 10^{-\kappa A}$ where $T_{A,\mathrm{obs}}(A)$ represents the antenna temperature observed through air mass A, which we take to be unity at the zenith; and T_A represents the antenna temperature that would have been seen through no atmosphere. The approximation $A = \sec z$ gives an excellent fit to the data for sec z less than 6($z < 80°$). The least squares best fit to all of our data yields the value

$$\kappa = 0.00437 \pm 0.00034.$$

For the sake of consistency, we reduce all measurements to outside the earth's atmosphere. All the data in the maps have been thus corrected. For data so treated we find that daily measurements of the S8 integral value were self-consistent to an accuracy of ±1 percent as measured against the calibrated noise tube operating at constant current and constant temperature. The absolute calibration of the noise tube itself was made in the laboratory using a liquid nitrogen load the adopted temperature for which has been appropriately corrected for input losses. This measurement has an uncertainty of 2 to 3 percent, and adds only a small uncertainty to the conversion to brightness temperature discussed in the next section.

CONVERSION TO BRIGHTNESS TEMPERATURE

In intercomparing HI surveys made by various observers, it is the brightness temperature T_B rather than the observed antenna temperature T_A that should be compared. T_B represents a physical quantity (brightness) in the sky, whereas T_A is dependent upon the brightness distribution of the source (or the standard region) and upon the properties of the antenna and receiver as well. For a given source each observer may be expected to find a different value of T_A because the properties of antennas differ.

Consider an extended HI cloud at velocity V having a brightness temperature distribution $T_B(\theta, \Psi, V)$, where θ and Ψ represent polar coordinates. We assume that the observation is made at a fixed velocity V and that a fixed observing velocity interval has been chosen. Then the observed line temperature T_A is given by

$$T_A = \frac{\int_{\Omega\ \text{source}} T_B(\theta, \Psi) \cdot F(\theta, \Psi)\, d\Omega}{\int_{4\pi} F(\theta, \Psi)\, d\Omega} \cdot \eta \tag{1}$$

where $F(\theta, \Psi)$ is the normalized antenna response pattern and η is the efficiency factor due to radiation losses. Combining eq. (1) with the usual relations for directivity D, gain G_o and effective area A_{eff}

$$D = \frac{4\pi}{\int_{4\pi} F(\theta, \Psi)\, d\Omega} \tag{2}$$

$$G_o = \eta D = \frac{4\pi}{\lambda^2} \cdot A_{\text{eff}} \tag{3}$$

$$\frac{G_o}{4\pi} = \frac{\eta}{\int_{4\pi} F(\theta, \Psi)\, d\Omega} \tag{4}$$

we find

$$T_A = \frac{G_o}{4\pi} \int T_B(\theta, \Psi) \cdot F(\theta, \Psi) \cdot d\Omega \tag{5}$$

Thus by measuring the antenna gain G_o by an independent method as described below, the problem of finding $T_B(\theta, \Psi)$ is reduced to solving the integral equation (5) knowing the source distribution and the antenna pattern. Methods by which this integral is evaluated for two special cases are given in the next two sections. Notice that the method takes advantage of the fact that the same loss factor η is present in both the gain measurement and the extended source measurement.

In order to calculate the correction factors K to convert from observed antenna temperature T_A to the brightness temperature, $T_B = KT_A$, it was necessary to determine the antenna pattern function over as much of the main beam and near-in sidelobe level as possible. It was found that by using the Cas A source as a signal that the pattern could be measured down to 33 db below the intensity at the center of the beam. The pattern was measured with observations spaced every 3′.2 arc over an area of 4° × 4°. The gain maximum G_o of the antenna was determined at the same time from the peak antenna temperature T_s measured for Cas A and M87 and using the known source flux S obtained from Baars, Mezger and Wendker (1965). The flux for Cas A was reduced by the 1.3 percent per year as recently determined by Scott, Shakeshaft and Smith (1969). The relation used is:

$$\frac{G_o}{4\pi} = \frac{2KT_s}{S\lambda^2}. \tag{6}$$

A value for $G/4\pi$ is found to be 6.67×10^3 and the corresponding value for the effective aperture of the 85-foot telescope is found to be 297 square meters.

a) *Disk distribution "observed" with the 85-foot telescope*

To evaluate the integral in equation (5) we first make some simplifying assumptions. We approximate the source function $T_B(\theta, \Psi)$ by a uniform bright disk. For a source distribution which has such a constant brightness temperature $T_{B,\text{disk}}$ over its diameter, the observed antenna temperature $T_{A,\text{disk}}$ is given by

$$T_{A,\text{disk}} = T_{B,\text{disk}} \cdot \frac{G_0}{4\pi} \int_{\Omega \text{ source}} F(\theta, \phi)\, d\Omega \tag{7}$$

This case thus reduces to integrating the antenna pattern out to the diameter of the disk source. Numerical integration of the data for the beam pattern has been performed for various disk sizes; in Figure 6 we plot

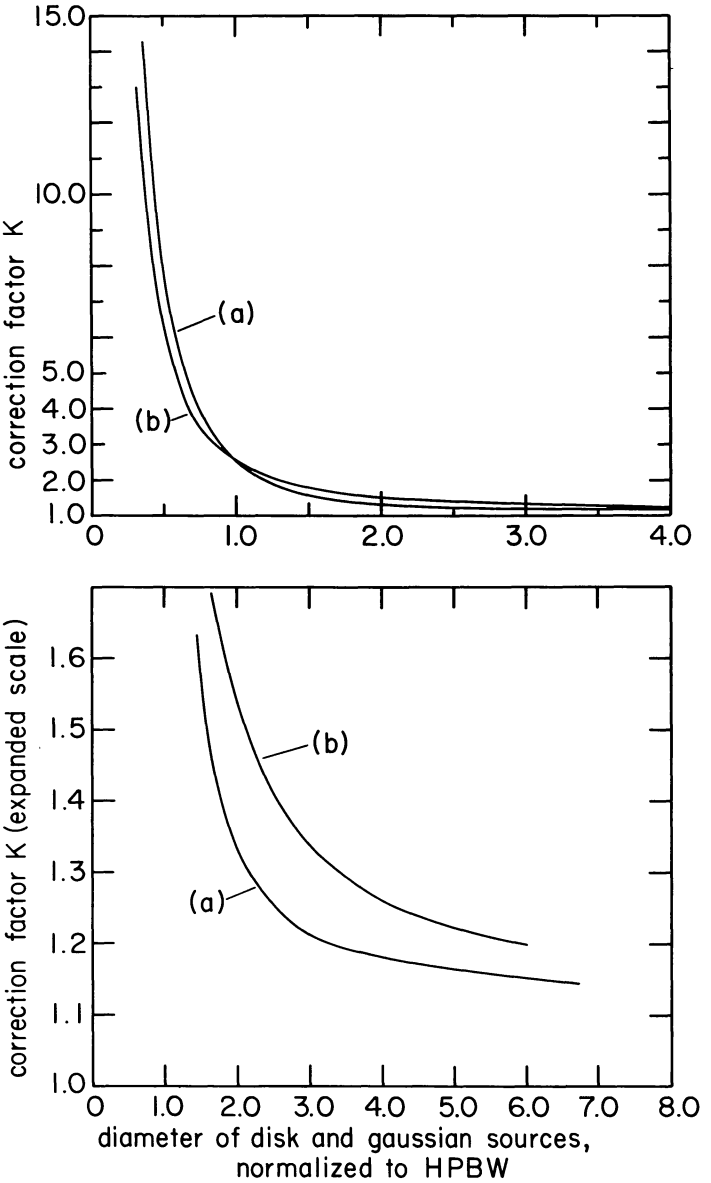

Figure 6. The correction factor K to be applied to the observed antenna temperature T_A to obtain the true brightness temperature, T_B where $T_B = KT_A$. Curve (a) applies to a disk distribution and (b) to a gaussian distribution when observed with the measured 85-foot telescope beam pattern. For convenience, the diameter of the disk source and the diameter of the gaussian source between the half-intensity points are measured in units of the HPBW of the telescope.

in curve (a) the conversion factor K, where $T_B = KT_A$. For convenience, the diameter of the disk source has been plotted in units of antenna HPBW.

b) *Gaussian distribution "observed" with the 85-foot telescope*

The next useful approximation is to assume that the brightness distribution of the source has a gaussian shape in two dimensions. For the case of a gaussian source distribution "observed" with the 85-foot telescope, we insert the gaussian weighting function

$$T(\theta, \Psi) = \exp^{-(\theta/1.2012\,\theta_o)^2} \tag{8}$$

into Equation (5) and again integrate numerically. This calculation yields the values of K plotted in Figure 6, curve (b). The diameter θ_o of the circular gaussian source between the half-intensity points is also given in units of the antenna HPBW.

Other weighting functions can of course be computed, but the use of these two widely differing functions in (a) and (b) above gives a measure of the uncertainty in K due to choice of source distribution. For source diameters near to unit HPBW the difference between the K factors for the two functions is surprisingly small. The difference increases as the diameter increases up to 2 HPBW; beyond, it decreases again. For very large diameters the two curves would be expected to converge to the same asymptotic value of K, corresponding to a source filling the full 4π steradians; K would then exceed 1.00 only by the resistive radiative losses of the system.

APPLICATION OF THE CORRECTION FACTORS TO THE STANDARD REGIONS

The direct application of the results to the standard regions is now considered. From the maps, regions S6, S8 and S9 are seen to cover at least 3–4° diameter so that the full measured correction factor of 1.145 is applied, assuming disk-like distributions. If the distributions are more gaussian-like, then the factor would become 1.20. If, however, the areas covered are much larger than 4°, then the correction factor is smaller but does not fall below 1.045, (corresponding to the radiation loss factor), and is still expected to be within the given error limit. Finally, taking into account the effect of systematic errors in the noise calibration system, errors in the point source calibration measurements and the uncertainty in the assumed source distribution, we estimate that the correction factor $K = 1.145 \pm 0.085$. For S7 the maps of figure 3 indicate a feature having a gaussian width of 3° for which the correction factor would be $K = 1.220 \pm 0.085$. However, the feature sits on top of structure which has a broader distribution in longitude, i.e. the distribution in ℓ is probably as much like a disk as that for the other regions. This would imply that K should be intermediate between 1.145 and 1.220 and, and value of 1.18 ± 0.085 has been adopted. The integrals and peak antenna temperatures in Table II are therefore multiplied by the corresponding factors to give the values in Table III. It is these values of corrected brightness temperatures which should be finally used for intercomparison between the various observations of the standard regions. The principal sources of uncertainty in the conversion of T_A to T_B, apart from systematic instrumental errors in internal calibrations, lie in our lack of knowledge of the antenna pattern outside the 4° area for which the beam was mapped, and also in our knowledge of the assumed source distributions. As new data become available from other surveys with different instruments especially with telescopes of greater resolving power, it is expected that the results will converge to give more accurate values for the brightness temperatures of these areas.

Table III
Integrated Line Strengths Corrected to Brightness Temperature Units and Peak Brightness Temperature

Region	Integrated intensity (°K km/sec)	T_B, peak (°K)
S6	299 ± 22	51 ± 4
S7	1132 ± 79	100 ± 7
S8	897 ± 66	72 ± 5
S9	953 ± 71	85 ± 6

ACKNOWLEDGEMENTS

The author wishes to acknowledge the interest and encouragement of Professor H. Weaver, Director of the Radio Astronomy Laboratory at the University of California in Berkeley. This work was in part supported by the National Science Foundation under grants GP-24611 and GP-30424X.

REFERENCES

Baars, J. W. M., Mezger, P. G., and Wendker, H., 1965, Ap. J, **142**, p. 122–134.
Goldstein, S. J., 1964, Proc. IEEE, **52**, 9.
Scott, P. F., Shakeshaft, J. R., and Smith, M. A., 1969, Nature, **223**, 1139.
van Woerden, H., 1970, Proceedings XIV I.A.U. Gen. Assembly (Reidel) Vol. XIV B, 217.
Weaver, H., Dieter, N. H., and Williams, D. R. W., 1968, Ap. J, Suppl., **146**, Vol. 16, p. 219.
Weaver, H., and Williams, D. R. W., 1973, Astron. and Astrophys. Suppl. **8**, 1.